

Mechanical and chemical properties of thick hybrid sol-gel silica coatings from acid and base catalyzed sols

A. Mehner · J. Dong · T. Prenzel · W. Datchary ·
D. A. Lucca

Received: 6 November 2009 / Accepted: 19 March 2010 / Published online: 31 March 2010
© Springer Science+Business Media, LLC 2010

Abstract Sol-gel silica hybrid coatings from acid and base catalyzed sols were examined. The sol precursors were tetraethyl orthosilicate (TEOS) and methyltriethoxysilane (MTES). It is generally accepted that the type of catalyst has a significant impact on the micro-structure of the resulting polysilicates. Weakly branched polymers are formed in acid catalyzed sols and highly branched, compact, particle like polymers are formed in base catalyzed sols. The mechanical and chemical properties of sol-gel derived silica coatings from acid and base catalyzed sols were studied as a function of the heat treatment temperature and time. Hardness and elastic modulus were measured by micro indentation measurements. The chemical composition of both types of coatings was characterized by X-ray photoelectron spectroscopy (XPS) and infrared spectroscopy (FTIR).

Keywords Silica hybrid coatings · Catalysis · Sintering · Hardness · E-modulus · XPS · FTIR

1 Introduction

Silica coatings from sols based on tetraethyl orthosilicate (TEOS: $\text{Si}(\text{OC}_2\text{H}_5)_4$) and methyltriethoxysilane (MTES: $\text{Si}(\text{CH}_3)(\text{OC}_2\text{H}_5)_3$) are interesting for many technical

applications, especially for optical [1] and electrical applications [2], for corrosion protection [3] and also for manufacturing of micro-structured optical molds, as shown in our previous papers [4, 5]. Silica coatings up to 17.3 μm were micro-structured by high precision fly cutting with diamond tools and successfully tested for injection molding of PMMA optical components with a micro-structured surface [6].

Numerous investigations on silica sols have shown that the chemical conditions as the molar ratio of water to alkoxide, the sol concentration, the type of solvent and the temperature cause modifications in the micro-structure of the resulting polysilicates [7]. The hydrolysis and the condensation of the silicon alkoxides precursors is catalyzed by acids or by bases since the reactivity of these alkoxides is very low. The type of catalyst has an impact on the growth mechanism of the polysilicates.

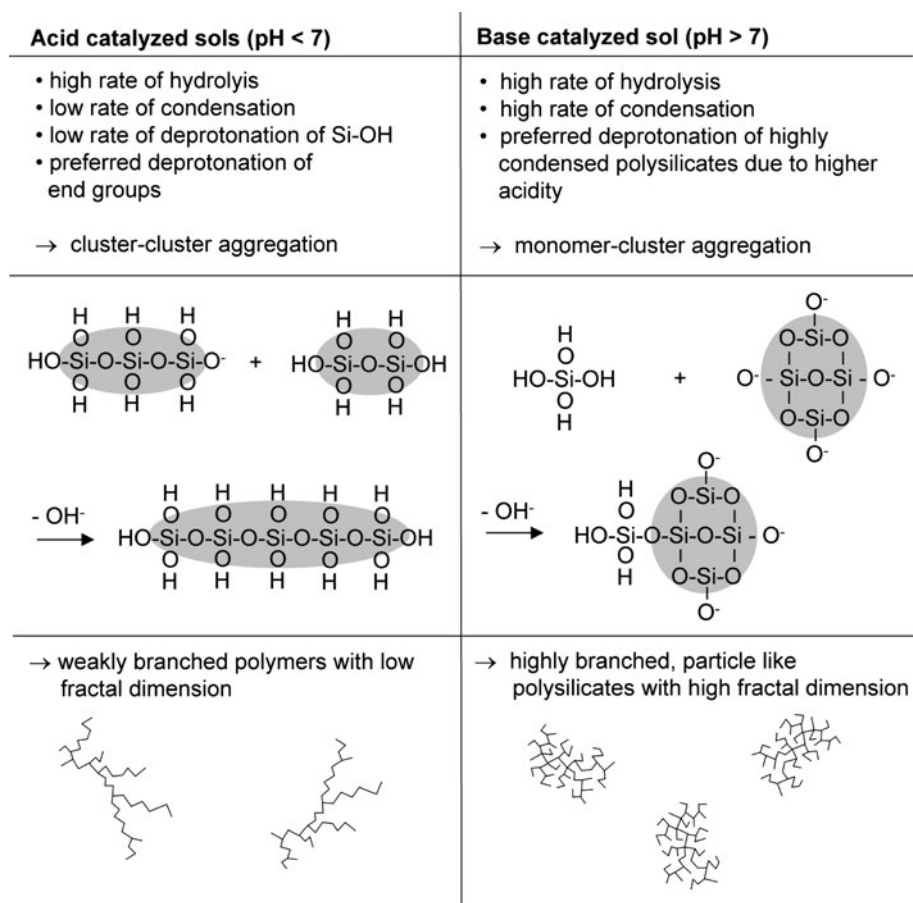
In acid catalyzed sols the growth of the polysilicates occurs by cluster-cluster aggregation resulting in weakly branched polymers, as shown in Fig. 1. For $\text{pH} < 6$ only few silanol groups are deprotonated and deprotonation preferentially occurs at the ends of the polysilicates since the acidity of the silanol groups is locally increased at the ends of polymers due to inductive effects. Thus, weakly branched polysilicates are formed in acid catalyzed sols [7, 8].

In base catalyzed sols the growth of the polysilicates predominately occurs by monomer-cluster aggregation resulting in highly branched, compact polymer clusters, as shown in Fig. 1. For $\text{pH} > 8$ the degree of deprotonation of the silanol groups $\equiv\text{Si}-\text{OH}$ is much higher compared to acid catalyzed sols. Especially, highly condensed polysilicates are deprotonated due to their higher acidity compared to that of the monomers [7]. The polysilicates become negatively charged due to the deprotonation. The electric

A. Mehner (✉) · J. Dong · T. Prenzel · W. Datchary
Stiftung Institut für Werkstofftechnik, Badgasteiner Str. 3,
28359 Bremen, Germany
e-mail: mehner@iwt-bremen.de

D. A. Lucca
School of Mechanical and Aerospace Engineering, Oklahoma
State University, 218 Engineering North, Stillwater,
OK 74078, USA

Fig. 1 The growth mechanisms of acid and base catalyzed silicate sols



repulsion between the charged polysilicates prevents cluster–cluster aggregation. Therefore, the polysilicates in base catalyzed sols preferentially condensate with neutral monomers by monomer-cluster aggregation which is leading to highly branched, compact polymer clusters [7, 8], as shown in Fig. 1.

The mechanical and chemical properties of coatings from acid and base catalyzed sols were investigated since it is expected that the different micro-structure of the gel may have an impact on the pyrolysis and the sintering behavior of the coatings.

2 Experimental

2.1 Sol synthesis

The sol precursors were tetraethyl orthosilicate (TEOS: $\text{Si}(\text{OC}_2\text{H}_5)_4$) and methyltriethoxysilane (MTES: $\text{CH}_3\text{Si}(\text{OC}_2\text{H}_5)_3$). For the acid catalyzed sols acetic acid (AcOH), water and ethanol (EtOH) were used [9, 10]. Polyvinyl pyrrolidone (PVP: $(\text{C}_6\text{H}_9\text{NO})_n$) was added to reduce the tendency of crack formation during the heat treatment [11]. The molar composition of sol A was TEOS: MTES:

$\text{AcOH:H}_2\text{O:PVP:EtOH} = 0.4:0.6:1:1:0.25:5$. A mixture of 74.8 mL ethanol, 4.7 mL dist. water and 16.2 mL acetic acid were vigorously stirred in a flask. While stirring the mixture 23.2 mL TEOS and 31.0 mL MTES were added. Finally, 7.2 g PVP powder was added and stirred into the slightly heated sol ($\approx 50^\circ\text{C}$).

The molar composition for the base catalyzed sol B was TEOS:MTES:NaOH: $\text{H}_2\text{O:EtOH} = 0.2:0.8:0.2:1:1:0.2$ [12]. A mixture of 98.8 mL MTES, 27.5 mL TEOS and 4.7 g NaOH were stirred for 12 h in a closed flask under non-streaming argon atmosphere. A mixture of 12.6 mL dist. water and 9.4 mL ethanol were stirred for 10 min and added drop wise to the TEOS-MTES-NaOH solution so that the temperature of the sol never exceeded 40°C .

Table 1 shows the molar composition of the acid and base catalyzed sols which were used for the coating experiments. The sols were stored in argon and the viscosity was measured 24 h after the synthesis using a spindle rheometer. The viscosity and the standard deviation were determined from a series of viscosity measurements at spindle frequencies from 2 to 15 s^{-1} . The temperature of the sols was $22 \pm 1^\circ\text{C}$ for all measurements. The measured viscosities of the sols A*, B and B* showed only slight dependency on the spindle frequency, as shown in

Table 1 Molar composition and viscosity of acid and base catalyzed TEOS-MTES sols used for the sol–gel deposition experiments

Sol	TEOS (mol)	MTES (mol)	AcOH (mol)	H ₂ O (mol)	EtOH (mol)	PVP (mol)	η (mPa s)
A	0.4	0.6	1.0	1.0	5.0	0.25	53 ± 7
A*	0.4	0.6	1.0	1.0	7.5	0.25	23 ± 3
B	0.2	0.8	0.2	1.1	0.2	–	16 ± 1.0
B*	Sol B diluted 1:1 with ethanol						

Fig. 2b indicating an almost Newtonian fluid behavior. The viscosity of sol A decreased with increasing spindle frequency indicating a typical shear-thinning effect of a polymeric liquid.

2.2 Sol deposition

The sol deposition was accomplished either by dip coating (Fig. 3a) onto polished stainless steel substrates (AISI 304, 20 × 40 × 1 mm³) for the micro indentation hardness measurements and by spin coating (Fig. 3b) onto polished silicon wafers ($\varnothing = 50$ mm, thickness $t = 0.5$ mm) for the chemical characterization of the coatings by XPS and FT-IR.

The withdrawal speed for the dip coating experiments was 10 cm min⁻¹ resulting in coating thicknesses in the range of 2–3 µm for the sols A* and B after the heat treatment. The coating specimens were left to dry in air for several minutes followed by a heat treatment in a preheated furnace at temperatures from 300 to 700 °C. The specimens were removed from the furnace after heating for 0.5 to 4 h and left in ambient air to cool down.

2.3 Mechanical properties

The coating thickness was measured by ball grinding experiments according to the European Standard ENV 1072-2 [13].

Fig. 2 **a** Spindle rheometer used for the viscosity measurements. **b** Measured viscosities of the acid and the base catalyzed TEOS-MTES sols versus the spindle frequency of the rheometer

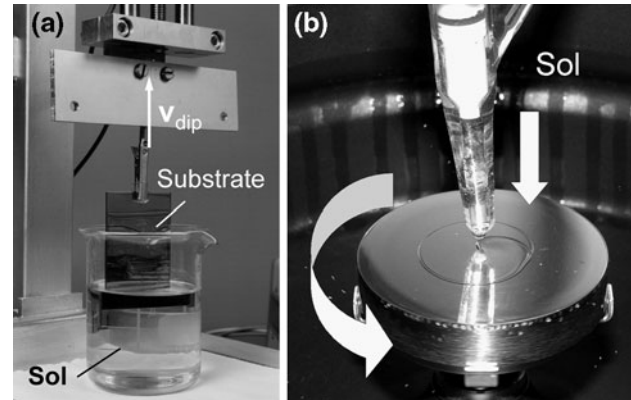
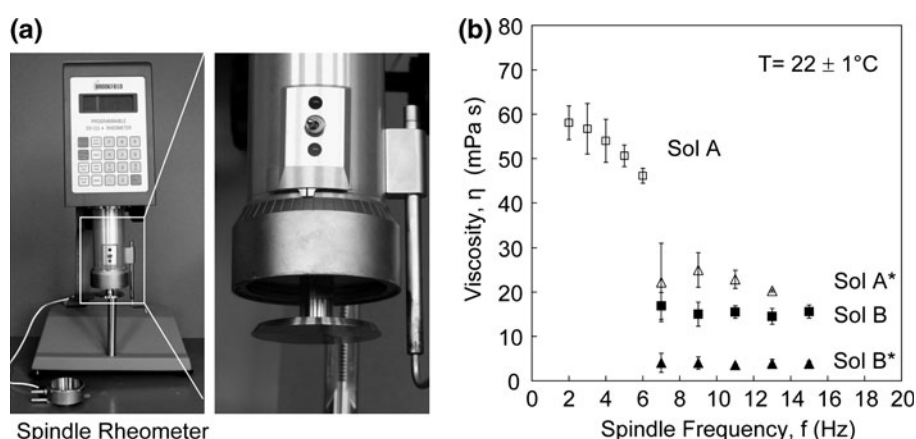


Fig. 3 **a** The dip coating of a stainless steel sheet **b** Spin coating of a steel disk

The indentation hardness H_{IT} and the reduced elastic indentation modulus E_r of the coatings were measured by micro indentation experiments using a commercial instrument with a Vickers diamond indenter. Figure 4 shows a typical load–displacement curve for a silica hybrid coating after heat treatment at 700 °C for 4 h.

For the indentation experiments the load was increased to the maximum load $F_{\max} = 10$ mN in 5 s. The holding time of F_{\max} was 2 s. No creeping occurred during this time. The indentation hardness H_{IT} and the reduced elastic modulus E_r were calculated using the equations shown in Fig. 4 [14].

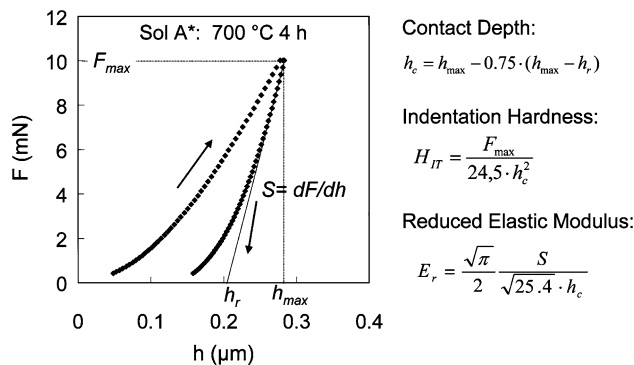


Fig. 4 A load displacement curve for a silica hybrid coating after heat treatment at 700 °C for 4 h. Indentation hardness H_{IT} and reduced elastic modulus E_r were calculated using the equations shown in the figure. These equations are valid for Vickers indenters [14]

The reduced elastic modulus E_r slightly differs from the real elastic modulus E_s of the specimen. The relation between E_r and E_s is given by the following equation: $1/E_r = (1 \approx v_i^2)/E_i + (1 - v_s^2)/E_s$ [15]. The elastic modulus and the Poisson's ratio of the diamond indenter tip are $E_i = 1140$ GPa and $v_i = 0.07$. The equation simplifies to: $1/E_r \approx (1 - v_s^2)/E_s$ for $E_r \ll E_i$, which is true for most materials. The sol-gel silica coatings have similar chemical compositions as soda lime glasses, which have Poisson's ratios from 0.18 to 0.30. For such Poisson's ratios the "real" elastic modulus E_s is about factor of 1.03 to 1.10 bigger than the measured reduced elastic modulus E_r . Only E_r values will be reported here because the Poisson's ratios of the tested coatings v_s are not known.

2.4 Chemical properties

The chemical composition of the coatings was measured by X-ray photo electron spectroscopy (XPS) using Mg K α radiation (1253.6 eV) and Al K α radiation (1486.6 eV). Al K α radiation was used for the coatings derived from the base catalyzed sol B* because these coatings contain sodium and the sodium Auger Na-KLL lines superimpose the carbon C 1s lines if Mg K α radiation is used. Thus, Al K α radiation was used for the coatings derived from sol B*.

Survey scans were recorded from 0 to 1100 eV with a step size of 1 eV. Detailed scans of the XPS lines of interest for the elements silicon (Si 2p), sodium (Na 1s), carbon (C 1s), oxygen (O 1s) and nitrogen (N 1s) were measured with a step size of 0.2 eV.

Argon ion etching was carried out to remove adsorbed surface contaminants like carbon dioxide (acceleration voltage: 3 kV, ion current: 1 μ A, sputter area: 0.75 cm $^{-2}$, sputter time: 480 s). Unfortunately, the ion etching changes the chemical composition of the coatings due to selective sputtering. Reference measurements on pure fused silica

(SiO₂) and silicon carbide (SiC) specimens were performed to quantify the effects of selective sputtering. The measured atomic ratio O/Si for fused silica was 2.0 before and 1.90 after ion etching. The C/Si ratio for silicon carbide specimens decreased from 1.0 to 0.85 after ion etching. These results indicate that oxygen and carbon atoms are sputtered more easily from the surface than the silicon atoms. The selective sputtering of carbon and oxygen was considered for the quantitative evaluation of the chemical composition. Energy shifts of the spectra up to ± 2 eV due to electrical charging of the insulating coatings during the measurement were corrected using the aliphatic carbon C 1s at ≈ 285 eV as an internal reference [16].

The hydrogen content of the coatings was measured by Elastic Recoil Detection (ERD) [17]. ERD measurements of the sol-gel coatings were performed using 3 meV He $^{2+}$ ions with a 30° detector position relative to the beam axis. A 14 μ m thick mylar film was placed in front of the detector to block the He $^{2+}$ ions. Hydrogen atoms of the coating scattered in the forward direction were detected by a silicon detector.

FT-IR spectroscopy was performed in order to study the influence of the heat treatment on the molecular properties of the coatings. Infrared spectroscopy experiments were accomplished with a commercial FT-IR spectrometer using an air-cooled LASER source emitting in the mid-IR. Specimens were mounted on a reflection unit with a fixed incident angle of 80° with respect to the surface normal of the specimen. The reflected beam was detected by liquid nitrogen cooled mercury-cadmium-telluride detector.

3 Results and discussion

3.1 Mechanical properties

The hardness and elastic modulus of coatings derived from sol A* and sol B were measured as a function of the heat treatment temperature and holding time. All coatings were crack-free and the coating thickness was between 2.0 and 3.1 μ m, depending on the heat treatment. The indentation depth was between 26 and 11% of the coating thickness, which is slightly above the 10% indentation depth rule according to Bückle [18]. Thus, the substrate is expected to have only a small influence on the indentation measurement results. The Fig. 5a and b show the indentation hardness H_{IT} and the reduced elastic modulus E_r of the coatings as a function of the heat treatment temperature for heating times of 0.5 and 4.0 h. Hardness and reduced elastic modulus increased with the heat treatment temperature. The hardness of the coatings from sol B exceeded that of the coatings from sol A* for all heat treatment temperatures from 300 to 700 °C. A maximum hardness of

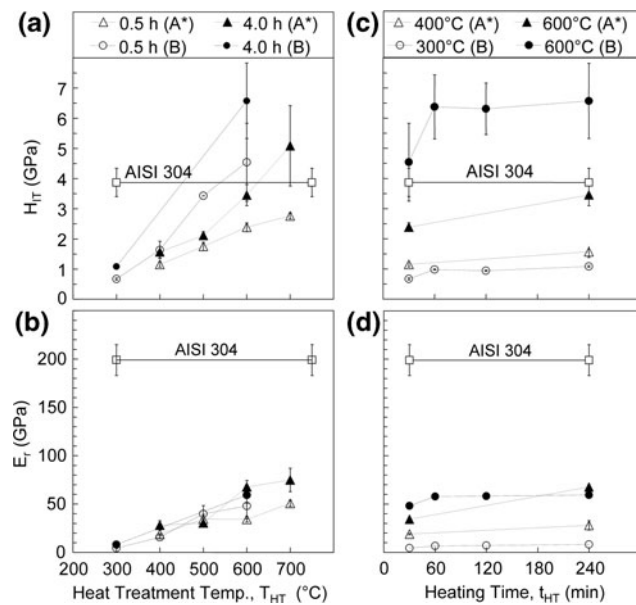


Fig. 5 **a** Indentation hardness H_{IT} and **b** reduced elastic modulus E_r of coatings from the acid catalyzed sol A* and the base catalyzed sol B as a function of the heat treatment temperature T_{HT} . (Error bars Standard deviation of 10 individual indentation experiments for each specimen.) **c** Hardness H_{IT} and **d** reduced elastic modulus E_r of the coatings versus heat treatment time t_{HT}

6.5 GPa was achieved for the coatings from sol B after heat treatment at 600 °C for 4 h, which is above the hardness of the stainless austenitic steel substrate. The big error bars for the hardness results after heat treatment for 4 h at 600 °C and above were due to small oxidation spots on the steel substrate below the coatings which had an influence on the local adhesion and thus on the local indentation measurement results.

The maximum E_r of the coatings was about 75 GPa, which is almost a factor of 3 below that of the steel substrate.

For soda lime glass Marschall et al. [19] reported a hardness of 5.5 GPa and an elastic modulus of 70 GPa. Thus, measured hardness and elastic modulus of the sol-gel coatings after heat treatment at 600 °C correspond well to the reported mechanical properties of soda lime glasses. The H/E ratio of the coatings varied from 0.056 to 0.070 which is between that reported for typical ceramics as Al_2O_3 with $H/E \sim 0.05$ and soda lime glasses with $H/E \sim 0.08$ [19].

The Fig. 5c and d show the indentation hardness H_{IT} and reduced elastic modulus E_r as a function of the heating time. The coatings derived from sol B showed an increase of hardness and modulus during the first 60 min. After 60 min hardness and elastic modulus remained almost constant indicating that the densification process of these coatings was almost finished after 60 min. The sol type has an impact on the sintering behavior of the coatings.

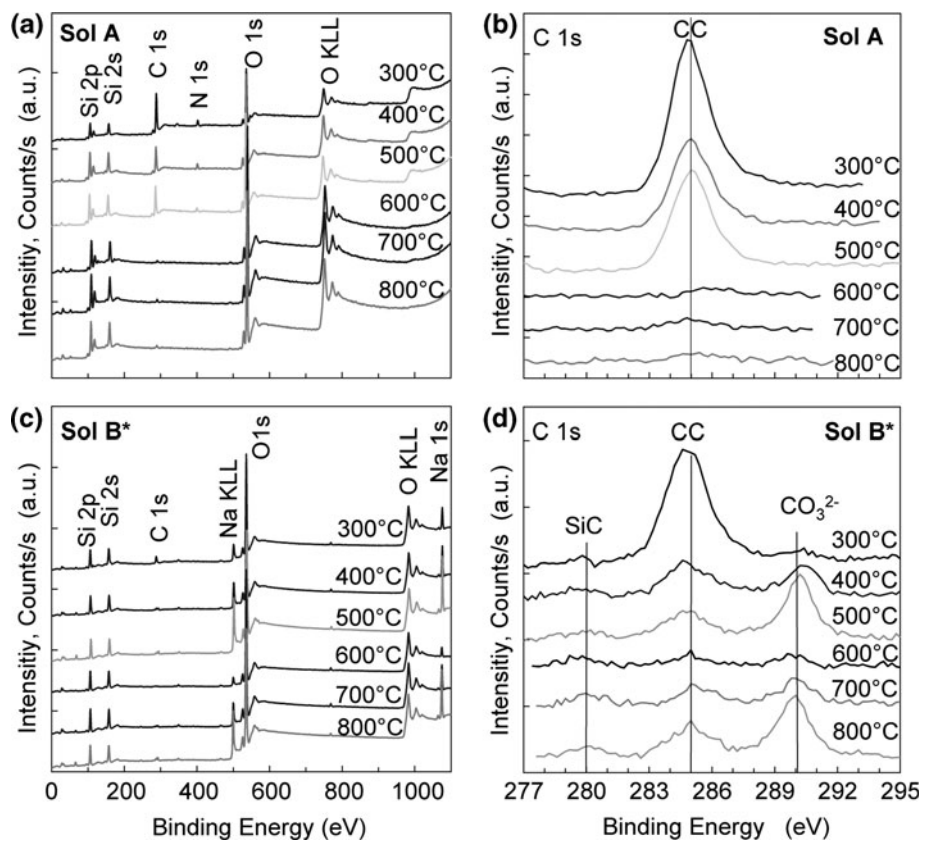
The higher hardness of the coatings from sol B is probably due to a higher density of the resulting xerogel films since base catalyzed sols contain compact, particle like polysilicates as shown in Fig. 1. Acid catalyzed sols form weakly branched polymers which preferentially aggregate in a 3-dimensional gel network with low density [7]. Secondly, the gel network of acid catalyzed sols is less condensed and contains more hydroxyl ($-OH$) and organic residues ($-OR$). These groups are known to constrain the densification processes [20]. Thirdly, the silica coatings from the base catalyzed sol B contain sodium which is known to reduce the glass transition temperature T_g and the softening temperature T_S . For pure silica quartz glass T_g is 1200 °C and T_S is 1740 °C. For a typical soda-lime glass containing ≈14% sodium T_g is 545 °C and T_S is 734 °C [21]. Thus, it is expected that the viscous sintering of sodium containing coatings derived from the (NaOH) base catalyzed sol B is faster than the viscous sintering of coatings from the acid catalyzed sol A* which do not contain any sodium.

3.2 Chemical composition

The chemical composition of the coatings was measured as a function of the heat treatment temperature. The coatings were deposited onto silicon wafers (\varnothing 50 mm, thickness, t : 0.5 mm) by spin coating at 1000 and 1500 rpm using the sols A and B*. Figure 6 shows XP survey spectra and detailed carbon C 1s spectra of both types of coatings after heat treatment at 300 to 800 °C. The coatings derived from sol A showed XPS lines of silicon, oxygen, carbon and nitrogen. The nitrogen is due to the organic additive, polyvinyl pyrrolidone ($\text{C}_6\text{H}_9\text{NO}_n$), which was added to reduce the tendency of crack formation [11]. The coatings derived from sol B* showed XPS lines of silicon, oxygen, carbon and sodium.

The C 1s lines of the coatings from sol A in Fig. 6b are due to aliphatic C-C and C=C bonds with a binding energy of 284.4 and 285.5 eV [22]. The intensity of these aliphatic carbon lines decreased as the heat treatment temperature was increased from 300 to 600 °C indicating a carbon loss due to oxidation. The C 1s spectra of the coatings derived from sol B* in Fig. 6d show besides aliphatic carbon at ≈285 eV additionally two other carbon lines at ≈290 eV and ≈280 eV. The 290 eV line is probably due to carbon in carbonates CO_3^{2-} with a binding energy of 290.6 eV [23]. The very weak signals at ≈280 eV are probably due to carbon in Si-C bindings [24]. It is suggested, that carbonates in the coatings from the sol B* were probably formed by a chemical reaction of the sodium hydroxide with carbon dioxide according to: $2\text{NaOH} + \text{CO}_2 \rightarrow \text{Na}_2\text{CO}_3$. The source of the carbon dioxide for this reaction could be from the air or from carbon dioxide which is

Fig. 6 **a** XP survey spectra and **b** carbon 1s spectra of coatings from the sol A after heat treatment at temperatures from 300 to 800 °C for 10 min (measured with Mg K α X-ray source), **c** XP survey spectra and **d** carbon 1s spectra of coatings from the sol B* after heat treatment at temperatures from 300 to 800 °C for 30 min (measured with Al K α X-ray source)



formed during the pyrolysis of the organic residues in the gel during the heat treatment.

The peak areas calculated from the least-squares fits of the measured XPS peaks were used for quantitative evaluation of the chemical composition of the coatings by the XPS sensitivity factor method.

The quantitative evaluation of the XP spectra in Fig. 7 shows the calculated atomic ratios H/Si, C/Si, O/Si, Na/Si, N/Si as a function of the heat treatment temperature for both types of coatings after heat treatment for 10 or 30 min. The H/Si ratios shown in Fig. 7 were determined by elastic recoil detection (ERD) [25].

Figure 7a shows the chemical composition of the coatings derived from the acid catalyzed sol A. The coatings contain a large amount of carbon for heat treatment at temperatures below 600 °C. The nitrogen due to the organic additive PVP was completely removed after heat treatment at 600 °C for 10 min. A significant part of the observed carbon and hydrogen in these coatings is due to the PVP since the PVP molecule contains 6 carbon and 9 hydrogen atoms per nitrogen atom. The O/Si ratio increased from 1.57 at 300 °C to 1.89 at 800 °C indicating a transition from an organic–inorganic hybrid material to almost inorganic SiO₂.

Figure 7b shows the chemical composition of the coatings derived from the base catalyzed sol B*. The carbon

and hydrogen content of these coatings was much lower than that for the coatings from sol A mainly since no PVP was used for sol B*. Similar XPS results were obtained by Sorarù and Nocuñ for silicon oxycarbide glasses [26, 27]. The O/Si ratio of the coatings from sol B* increased from about 1.9–2.7. O/Si ratios above 2 indicate the formation of other oxides besides SiO₂. The C 1s spectra in Fig. 6d showed carbonate CO₃²⁻ formation which is probably the source for the additional oxygen. The Na/Si ratio of the base catalyzed coatings increased from about 0.2 to 1.0 between 300 and 500 °C. At 600 °C a significant decrease of the sodium content was observed. It is speculated that this effect is caused by decomposition of sodium carbonates at the surface of the specimens.

Figure 8 shows FTIR spectra of coated silicon wafers. The spectra were measured in reflection mode. Both types of coatings show similar FTIR spectra. The IR peaks at 1060 and 1160 cm⁻¹ are attributed to the transverse optical (TO) and the longitudinal optical component (LO) of the asymmetric stretching vibration of Si–O–Si [28]. These peaks shift to higher wave numbers as the heat treatment temperature is increased. Higher wave numbers correspond to higher vibration frequencies of the Si–O–Si chains. It is suggested that the higher vibration frequencies are caused by the cross-linking of the Si–O–Si chains. The intensity of the LO peak at 1160 cm⁻¹ is correlated to the bonding

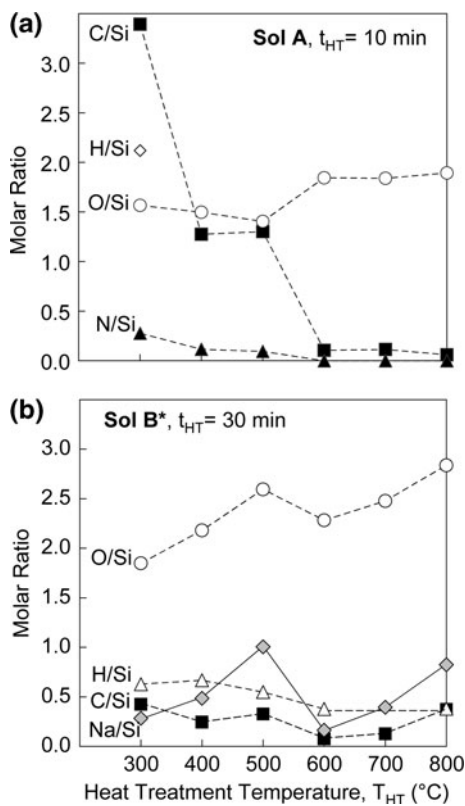


Fig. 7 Measured atomic ratios C/Si, O/Si, H/Si, N/Si and Na/Si as a function of the heat treatment temperature for coatings **a** from the acid catalyzed sol A and **b** the base catalyzed sol B*. The heating time was 10 min for the A coatings and 30 min for the B* coatings

angle and the bonding length of Si–O next to the surface of gel pores [28]. The IR-peak at 1277 cm^{-1} is due to the symmetric stretching vibration of the CH_3 group in $\text{Si}-\text{CH}_3$ [29]. The peak position does not change as the heat treatment temperature is increased from 300 to $800\text{ }^\circ\text{C}$, but the peak intensity reduces significantly. The SiCH_3 groups of the MTES molecule are stable up to $400\text{ }^\circ\text{C}$ [30]. The disappearance of the SiCH_3 peak above $600\text{ }^\circ\text{C}$ for the acid and above $500\text{ }^\circ\text{C}$ for the base catalyzed coatings is caused by pyrolysis and oxidation of the methyl groups at temperatures above $500\text{ }^\circ\text{C}$.

4 Conclusions

The mechanical and chemical properties of sol–gel silica coatings from acid and base catalyzed silica sols were examined as a function of the heat treatment temperature and the heating time. Hardness and elastic modulus increased with the heat treatment temperature from 300 to $700\text{ }^\circ\text{C}$ and with the heating time from 0.5 to 4 h for both types of coatings. The coatings from a base catalyzed sol showed higher hardness and elastic modulus compared to

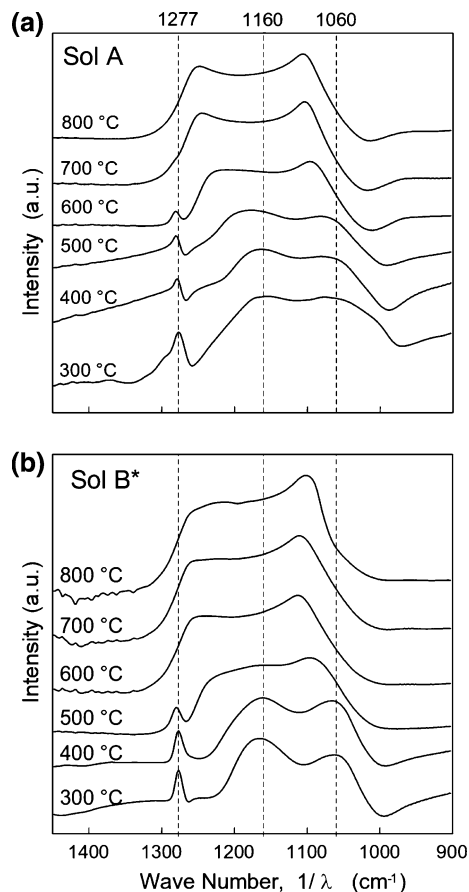


Fig. 8 FTIR spectra of coatings derived from **a** the sol A and **b** from the sol B* after heat treatment at 300 to $800\text{ }^\circ\text{C}$ for 10 min

those from an acid catalyzed sol after the same heat treatment. The different hardness and elastic modulus of both types of coatings is probably due to differences in the sintering behavior of the resulting xerogels. Three mechanisms were proposed to explain these differences. Firstly, base catalyzed sols contain compact particle like polysilicates that aggregate in a dense xerogel, whereas acid catalyzed sols form weakly branched polysilicates that preferentially aggregate in a 3-dimensional gel network with lower density [7]. Secondly, the gel networks of acid catalyzed sols are less condensed and contain more hydroxyl ($-\text{OH}$) and organic residues ($-\text{OR}$). These groups are known to constrain the densification processes [20]. Additionally, the chemical characterization revealed that the coatings derived from the acid catalyzed sol contain much more aliphatic carbon than the coatings from the base catalyzed sol. The higher carbon content of the acid catalyzed coatings probably constrains the densification process. Thirdly, the silica coatings from the base (NaOH) catalyzed sol contain sodium which is known to reduce the glass transition temperature T_g and the softening temperature T_S [21]. Thus, it is expected that the viscous sintering

velocity of sodium containing coatings is faster than the viscous sintering of coatings from the acetic acid catalyzed sol which do not contain sodium.

The XPS characterization of the coatings revealed that the coatings from the base catalyzed sol contain large amounts of carbonates (CO_3^{2-}) additionally to the aliphatic carbon and also small amounts of carbidic bound carbon as Si-C. The carbonates in these coatings were probably formed by a chemical reaction of the sodium hydroxide with carbon dioxide according to $2\text{NaOH} + \text{CO}_2 \rightarrow \text{Na}_2\text{CO}_3$. The source of the carbon dioxide for this reaction could be from the air or from carbon dioxide emerged during the oxidation of the organic residues in the gel during the heat treatment. To avoid carbonate formation other base catalysts as ammonia hydroxide NH_4OH should be used.

Acknowledgments This work is part of the Transregional Collaborative Research Centre SFB/TR4 “Process Chains for the Replication of Complex Optical Elements”. The support of the Deutsche Forschungsgemeinschaft (DFG) through the SFB/TR4 and the National Science Foundation through Grant Nos. OISE-0352377 and OISE-0128050 is gratefully acknowledged. The Los Alamos National Laboratory portion of this work was supported by the Department of Energy, Office of Basic Energy Sciences, and the Center for Integrated Nanotechnologies, a US Department of Energy, Office of Basic Energy Sciences user facility at Los Alamos National Laboratory (Contract DE-AC52-06NA25396) and Sandia National Laboratories (Contract DE-AC04-94AL85000).

References

- Zhang X, Qian M, Zeng X, Zhao Z et al (2008) J Sol Gel Sci Technol 45:103
- Shilova OA, Hashkovsky SV, Tarasyuk EV (2003) J Sol Gel Sci Technol 26:1131
- Chou TP, Chandrasekaran C, Cao GZ (2003) J Sol Gel Sci Technol 26:321
- Datchary W, Mehner A, Zoch H-W, Lucca DA, Klopstein MJ, Ghisleni R, Grimme D, Brinksmeier E (2005) J Sol Gel Sci Technol 35:245
- Mehner A, Zoch H-W, Datchary W, Pongs G, Kunzmann H (2006) CIRP Ann 55(1):589
- Mehner A, Dong J, Hoja T, Prenzel T, Mutlugünes Y, Brinksmeier E, Lucca DA, Klaiber F (2010) Key Eng Mater 438:65–72
- Brinker CJ, Scherer GW (1990) Sol-gel science: the Physics and Chemistry of sol-gel processing, Chap. 3. Academic Press Inc, San Diego
- Iller RK (1979) The chemistry of silica. Wiley, New York
- Schmidt H (1984) Mat Res Soc Symp Proc 32:327
- Villegas MA, Aparicio M, Duran A (1997) J Non Cryst Solids 218:146
- Kozuka H, Kajimura M, Hirano T et al (2000) J Sol Gel Sci Technol 19:205
- Menning M, Jonschker G, Schmidt H (1997) German Patent DE 197 14 949 A1
- Mehner A, Datchary W, Bleil N, Zoch H-W, Klopstein MJ, Lucca DA (2005) J Sol Gel Sci Technol 36:25
- Pethica JB, Hutchings R, Oliver WC (1983) Philos Mag A 48:593
- King RB (1987) Int J Solid and Struct 23:1657
- Briggs D (1998) Surface analysis of polymers by XPS and static SIMS. Cambridge University Press, Cambridge
- L'Ecuyer JL, Brassard C, Cardinal C et al (1976) J Appl Phys 47:381
- Bückle H (1959) Metallurgical Rev 4:49
- Marschall DB, Noma T, Evans AG (1982) J Am Ceram Soc 65(10):175
- Scherer GW (1997) J Sol Gel Sci Technol 8:353
- Kim KD, Ondarec G (1995) J Mat Sci Let 14:455
- Roy SS, McCann R, Papakonstantinou P et al (2005) Thin Solid Films 482:145
- Lukaszewicz JP (1997) J Mater Sci 32:6063
- Moulder JF, Stickle WF et al (1992) Handbook of x-ray photoelectron spectroscopy. Perkin-Elmer Corp, Minnesota
- Lucca DA, Ghisleni R, Nastasi M et al (2007) Nucl Instrum Methods Phys Res B 257:577
- Soraru GD, d'Andrea G, Glisenti A (1996) Mater Lett 27:1
- Nocuñ M, Leja E, Jedliński J, Najman J (2005) J Mol Struct 744–747:597
- Almeida RM, Pantano CG (1990) J Appl Phys 68(8):4225
- Socrates G (1980) Infrared characteristic group frequencies. Wiley, Chichester
- Murtagh MT, Shahriari MR, Krihak M (1998) Chem Mater 10:3862